

Experiment study on the bonding quality and shear performance of composite glulam manufactured by densified Chinese fir

Panpan Ma^a, Xin An^a, Bin Zhou^a, Shuo Wang^a, Xinran Li^a, Jianzhang Li^b, Jinqiu Xie^a, Zeli Que^{a,*}

^a College of Material Science and Engineering, Nanjing Forestry University, Nanjing, Jiangsu 210037, China

^b College of Material Science and Engineering, Beijing Forestry University, Beijing 100083, China

ARTICLE INFO

Keywords:

Chinese fir
Densified wood
Glulam
Bonding quality
Shear strength

ABSTRACT

Chinese fir is a vital softwood species in South China, dominates stock volume but faces limitations in structural applications due to low density and poor strength. To enhance its structural use and increase its value, this study manufactured four layers composite glulam using densified fir for the outer laminates and untreated fir for the inner layers. Bonding quality was assessed through glue-line delamination and shear tests, while shear performance was evaluated via three-point bending tests with a span-to-depth ratio of 2. Results showed that densification of the outer laminates significantly improved bonding quality and load capacity. The total and maximum delamination of composite glulam were both under 5 %, much lower than those in normal glulam. The glue-line shear test indicated a mean strength of 6.62 MPa, 27.8 % higher than normal glulam. Both delamination and shear tests confirmed that the composite glulam met GB/T 26899-2022 standards. The bending tests demonstrated a 21.51 % increase in shear strength compared with normal glulam, with a mean value of 4.85 MPa. Most specimens exhibited shear failure near the neutral axis, although one specimen showed cracking at a point one-quarter of the height from the bottom of the beam, suggesting the need to consider shear stress variations across the laminates in future designs. These findings illustrated the effect of densified outer laminates and underscored the viability of producing structural glulam using Chinese fir.

1. Introduction

Glulam is an engineered wood product composed of wood laminations bonded along the grain. It retains the renewable nature and aesthetic appeal of natural wood while offering advantages such as enhanced load-bearing capacity and minimized effects from natural growth defects like knots. These benefits make glulam a key structural material in modern timber construction, providing a viable alternative to steel and concrete (Harte, 2017). However, the development and application of glulam in China face significant challenges due to limited domestic wood resources. Current glulam production in China relies heavily on imported wood, revealing a substantial gap between local timber supply and demand (Ou et al., 2023). To address this issue, exploring the use of domestic plantation wood for glulam production is essential.

Chinese fir (*Cunninghamia lanceolata* (Lamb.) Hook.) is a key softwood species in South China, with a stock volume of 755 million m³,

accounting for nearly one-third of plantation forests (National Forestry and Grassland Administration, 2019). Currently, it is primarily used for low-value products like chipboard, fiberboard, and paper (X. Wang et al., 2018) largely due to defects like low density, poor strength, and dimensional instability resulting from rapid growth. As plantation reserves peak, there is an urgent need for sustainable methods to enhance its high-value applications (Kong et al., 2024). However, with a density typically below 0.4 g/cm³, Chinese fir lacks sufficient load capacity for structural applications, which is often directly related to wood density. The low density and compressive strength of Chinese fir can lead to plastic deformation at the supports when used as beams, resulting in eccentricities and load redistributions within the structure. This may overstress certain parts of the structure and ultimately affect its overall stability.

To address this, densification has proven to be an effective modification technique for enhancing the density and mechanical properties of low-density wood, transforming it into high-performance products (J.

* Corresponding author.

E-mail address: zeliq@njfu.edu.cn (Z. Que).

<https://doi.org/10.1016/j.indcrop.2025.120565>

Received 25 October 2024; Received in revised form 3 January 2025; Accepted 16 January 2025

Available online 24 January 2025

0926-6690/© 2025 The Authors. Published by Elsevier B.V. This is an open access article under the CC BY-NC license (<http://creativecommons.org/licenses/by-nc/4.0/>).

Wang et al., 2018). Thermo-mechanical densification, achieved through a combination of heat, moisture, and mechanical pressure, is an eco-friendly, cost-efficient process that improves wood's dimensional stability and mechanical properties, making it suitable for engineered wood products like glulam and cross-laminated timber (Sotayo et al., 2020; Srivaro et al., 2022). Utilizing densified wood with enhanced density and mechanical properties as the outer laminates, while using untreated wood as the inner laminates, is a cost-effective approach that theoretically maintains the mechanical properties of glulam. This design leverages the fact that when a glulam beam is subjected to flexural load, the maximum bending stresses happen at the topmost and bottommost points (maximum distances from the neutral axis) of glulam layers rather than the middle layer. However, glulam beams are also subjected to shear loads, which are greatest along the neutral axis, where the untreated wood is located (Ido et al., 2009). Especially in short beams, shear stress often governs the design rather than bending stress (Franke et al., 2015). Given that untreated wood typically has lower shear strength, there is a risk of shear failure in composite glulam. While previous studies have explored the use of densified wood in glulam production (Hajihassani et al., 2021; Liew et al., 2022), however, few have investigated the properties of composite glulam fabricated from densified and untreated wood. Therefore, it is essential to study the shear performance of composite glulam to determine whether it meets the structural demands for construction.

In all glued engineered wood products (EWPs), the characteristics of the interfacial adhesive bond play a crucial role in determining product integrity and quality (J.B. Wang et al., 2018). Bonding quality is closely related to surface roughness and wood porosity (Söğütlü, 2017). The densification process, which causes the collapse of cell lumens and fiber pores in the wood, reduces porosity and smooths the wood surface (Liu et al., 2018), significantly affecting the bonding quality of glued EWPs. Some studies suggest that the smoother surface of densified wood can lead to lower bonding quality, as it may hinder adhesive penetration into the capillaries of wood, resulting in reduced shear strength in glue-line shear tests and an increased delamination ratio of the glue lines (Nandika et al., 2021). However, other research has shown that densified glulam can exhibit higher shear resistance compared to untreated glulam, due to the enhanced mechanical properties, particularly shear strength, gained through the densification process (Liew et al., 2022). To ensure the bonding durability and quality of glulam made with densified wood, it is essential to thoroughly investigate the effects of the densification process on glulam bonding performance.

This study hypothesizes that densifying the outer laminates of Chinese fir will enhance shear strength, alter the failure mode of short beams, and improve glue-line shear strength. These properties are strongly correlated with compression and shear resistance, which can be improved through densification. While the effects of densification on bonding quality have shown mixed results in previous studies, it is anticipated that by carefully controlling densification parameters, potential negative impacts on bonding can be minimized. The key issues addressed in this study are as follows:

- The impact of densifying the outer laminates on the bonding performance of Chinese fir glulam.
- The contribution of densified outer laminates to the shear performance of glulam beams.
- Whether the performance of Chinese fir composite glulam meets standard requirements.

The objective of this study is to explore the effects of outer laminate densification on the mechanical properties and structural performance of Chinese fir glulam, specifically focusing on shear strength and bonding durability. By evaluating these effects, the study aims to verify whether composite Chinese fir glulam meets structural requirements, thereby enhancing the commercial value of Chinese fir through its increased suitability for structural applications.

2. Materials and methods

2.1. Raw materials

Chinese fir [*Cunninghamia lanceolata* (Lamb.) Hook.] was harvested from plantations in Jiangxi province, China, was utilized as the raw material for this study. The trees were 15 years old. After air drying, they were divided into two groups. The first group was sawn into dimensions of 2000 mm (L) 60 mm (W) 40 mm (R) for subsequent densification treatment. The second group was sawn into dimensions of 2000 mm (L) 60 mm (W) 25 mm (R) without undergoing any modification treatment. The table saw (CS 70 EB CN, Festool Deutschland, Germany) were used to split the wood. Visual grading was performed to identify and exclude timbers with significant defects such as cracks, warping, insect infestation, or decay. Only pieces with small, isolated knots were selected, ensuring that the total knot diameter within a 150 mm length did not exceed 12 mm, and that the ratio of the total knot diameter to the width of the wood edge was less than 20 %, in accordance with the Chinese structural glulam manufacturing standard (Standardization Administration of China, 2022). Both groups of timber were then conditioned in a controlled environment at a temperature of 20 °C and a relative humidity of 65 %. Following conditioning, each sawn timber was further processed into 4 timber boards with a length of 400 mm, while maintaining the original cross-sectional dimensions in preparation for subsequent treatment. The density and moisture content of the Chinese fir timber were determined in accordance with GB/T 1927.5 (Standardization Administration of China, 2021a) and GB/T 1927.4 (Standardization Administration of China, 2021b) standards, respectively. The average density and moisture content of the natural Chinese fir were found to be 0.385 ± 0.031 g/cm³ and 14.51 ± 1.29 %.

2.2. Preparation of the composite Chinese fir glulam

2.2.1. Pre-heating treatment

Fig. 1 shows the schematic image of densification. The densification process, comprising heating, pressing, and pressure-holding phases, was performed using a hot press (XLB-1MND, YADONG GROUP, China) in the radial direction.

To ensure the wood structure was adequately softened before mechanical pressing, a pre-heating treatment was conducted. This step is essential for achieving densification without causing cell wall breakage (Kutnar et al., 2015). Both the pre-heating temperature and moisture content of the wood are crucial, as the glass transition temperature of wood decreases with increased moisture content, significantly influencing its softening behavior. Additionally, the duration of pre-heating is important: too long a duration may lead to excessive degradation of the wood components. These factors were optimized in previous studies (Ma et al., 2023). The pre-heating was carried out at a temperature of 120 °C, for a duration of 20 min, with the moisture content of the wood adjusted to 50 %. The target moisture content was achieved by soaking the specimens in distilled water at room temperature until the difference between the mass obtained through the weighting operation and the mass calculated according to Eq. (1) was within 0.5 g. Specimens at the target moisture content were then placed in contact with hot platens which were already heated to the specified temperature, and softened under a load of less than 0.5 MPa for the set duration.

$$m_1 = \frac{(1 + W_1)m_0}{W_0} \quad (1)$$

Where: m_1 is the mass of specimens at the target level of moisture content, in g; W_1 is the target moisture content, in %; m_0 is the mass of specimens prior to soaking, in g; W_0 is the moisture content of the specimens prior to soaking, in %.

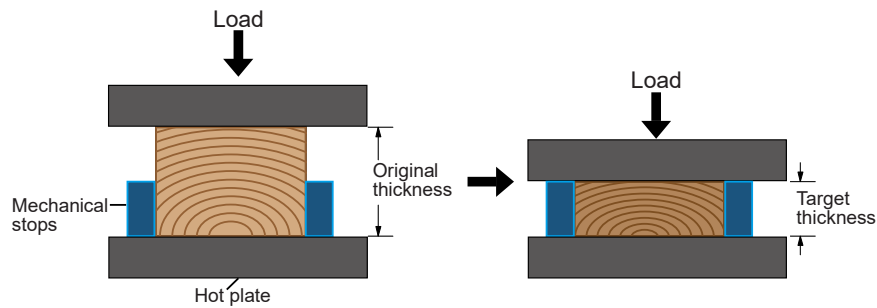


Fig. 1. Schematic image of densification.

2.2.2. Densification process

Following the pre-heating treatment, the densification process was performed using parameters from previous studies: a compression ratio of 50 %, a pressing temperature of 140 °C, a compression pressure of 6 MPa, and a pressure holding time of 3 h. The platen temperature was increased to 140 °C at an average heating rate of 1.9 °C/min following the completion of the pre-heating treatment (Ma et al., 2023). A segmented pressurization method was applied to prevent cracking in the densified wood, with a 1-minute interval at 2 MPa pressure. The thickness of the densified Chinese fir was monitored using mechanical stops, achieving a target thickness of 20 mm at a pressure of 6 MPa. Once the designated pressure and target thickness were reached, the specimens were maintained under pressure for 3 h to stabilize the deformation. This relatively long pressure-holding time allowed sufficient solidification of the lignin-hemicellulose matrix before the compression load was released, effectively reducing spring-back (Paul et al., 2024). During the load-holding phase, the hot platens were allowed to cool to room temperature. The entire densification process is illustrated in Fig. 2. The average density and moisture content of densified Chinese fir was found to be 0.678 ± 0.036 g/cm³ and 13.90 ± 1.42 %.

2.2.3. Scanning electron microscopy (SEM) examination

For microstructure observation, samples with dimensions of 5 mm (L) × 5 mm (W) × 5 mm (R) were cut from both untreated and densified Chinese fir specimens. The surfaces of the samples were smoothed and flattened. The samples were dried to a completely dry state and then fixed on an aluminum sample holder using conductive adhesive tape. Vacuum-gold coating was applied via ion sputtering (SBC-12, Beijing Zhongke Keyi, China). After coating, the samples were transferred to SEM (Phenom XL, Phenom Scientific Instruments, China) for imaging.

2.2.4. Glulam manufacturing

The four-layer composite glulam with dimensions of 400 mm (L) 55 mm (W) 80 mm (R) was fabricated using densified Chinese fir for the upper and lower laminates, while non-densified Chinese fir was used for the core laminates. Normal glulam, serving as the control specimens,

was also produced from non-densified Chinese fir. The dimensions of the specimens and a schematic representation of the glulam manufacturing process are shown in Fig. 3.

To mitigate spring-back and set-recovery effects, wood softening and pressure-holding phases were applied before and after densification. The densified laminates were then planed using a four-side planer to achieve a uniform thickness of 20 mm, eliminating potential dimensional changes and removing thermally degraded fibers from the surface. The untreated laminates were planed in the same manner to ensure consistent thickness across all specimens. Before gluing, the surfaces were thoroughly cleaned to remove any dust or debris. The laminates were bonded using PUR adhesive (200C-B, BASF, China), which was manually applied with rollers to one face to ensure an even spread. The adhesive application rate was controlled by measuring the adhesive weight, applying 250 g of PUR adhesive per square meter of surface area. The laminates were then assembled and pressed under a load of 1.0 MPa for 24 h using a hot press. After pressing and initial curing, the glulam beams were allowed a post-pressing stabilization period of 24 h to ensure complete bonding and stabilize the wood's moisture content. The environmental temperature and relative humidity during glulam manufacture were 11 °C and 62 %, respectively. 6 replicates were prepared for both the composite and control glulam specimens. The main processes of glulam manufacturing are shown in Fig. 4.

2.3. Tests for bonding quality and durability

2.3.1. Delamination test procedure

The delamination specimens, with dimensions of 75 mm (L) × 55 mm (W) × 80 mm (T), were cut from both normal and composite glulam, maintaining a 50 mm distance from the edge of the glulam. A total of 12 specimens were subjected to soaking and boiling delamination tests in accordance with GB/T 26899 (Standardization Administration of China, 2022).

The soaking delamination test was conducted as follows: specimens were soaked in water at room temperature for 24 h and then placed in a drying oven at 70 °C. When the specimens' weight reached 100–110 % of their pre-soaking weight, the delamination length was measured. For the boiling delamination test, the specimens were soaked in boiling water for 4 h, followed by immersion in water at room temperature for 1 h. Afterward, the specimens were dried in the same manner as the soaking delamination test, and the delamination length was measured. Each test involved repeating the soak-dry cycle twice for the soaking delamination test and the boil-soak-dry cycle twice for the boiling delamination test to meet the requirements for service class 3 usage, which corresponds to outdoor environments with high humidity. The total delamination percentage and maximum delamination percentage were calculated using Eqs. (2) and (3).

$$P_t = \frac{l_{tot}}{L_{tot}} \times 100\% \quad (2)$$

Where: P_t is the total delamination percentage, in %; l_{tot} is the total

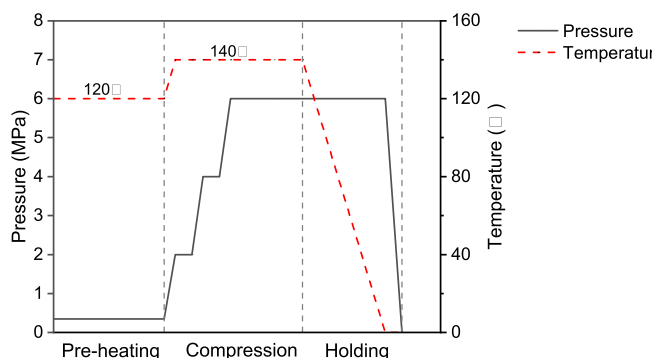


Fig. 2. Schematic image of segmented pressurization process.

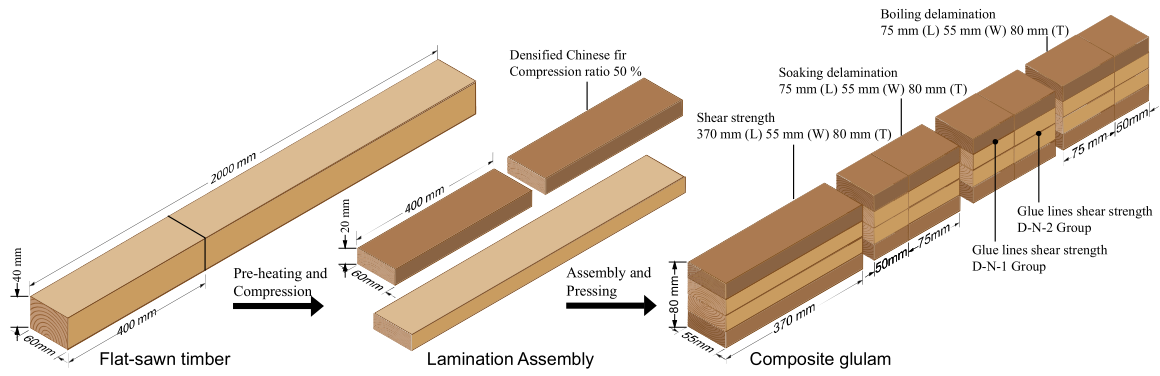


Fig. 3. Schematic diagram for specimen preparation.



(a) Air-drying the sawn lumbers



(b) planed laminates



(c) bonding laminates

Fig. 4. Processes of glulam manufacturing.

delamination length, in mm; and L_{tot} is the sum of the perimeters of all glue-lines in a delamination specimen, in mm.

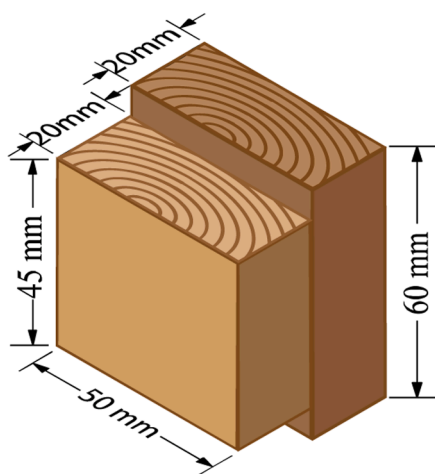
$$P_m = \frac{l_{max}}{L_{glueline}} \times 100\% \quad (3)$$

Where: P_m is the maximum delamination percentage, in %; l_{max} is the maximum delamination length, in a single glue-line, in mm; and $L_{glueline}$

is the length of the glue-line where delamination occurred, in mm.

2.3.2. Glue-line shear strength test

The shear test specimens were prepared from both normal and composite glulam. In the normal glulam, the bonding interfaces were labeled as N-N-1 for the outer-to-inner laminate and N-N-2 for the inner-to-inner laminate, while in the composite glulam, these interfaces were



(a) specimen dimensions



(b) test setup

Fig. 5. Schematic diagram of block shear test specimen and test device.

labeled as D-N-1 and D-N-2, respectively. Each type of specimen had six replicates, making a total of 24 specimens subjected to block shear tests according to GB/T 50329 (Ministry of Housing and Urban-Rural Development of the People's Republic of China, 2012). The tests were performed using a universal testing machine (UTM4304, SUNS, China), with the load applied continuously at a test speed of 5 mm/min. The specimen dimensions and schematic of the test setup are shown in Fig. 5 (a) and (b), respectively. Each test was automatically stopped once the specimen reached the maximum shear load, and the shear strength was calculated using Eq. (4). The wood failure percentage was determined based on Eq. (5).

$$f_{v,block} = \frac{Q_u}{A_v} \quad (4)$$

Where: f_v is the glue-line shear strength, in MPa; Q_u is the maximum load, in N; and A_v is the area bearing the shear load, in mm^2 .

$$P_v = \frac{A_t}{A_v} \times 100\% \quad (5)$$

Where: P_v is the wood failure percentage, in %; A_t is the area of wood failure, in mm^2 ; A_v is the total bonding area, in mm^2 .

2.4. Tests for shear performance of glulam short beams

2.4.1. Test program and setup

To evaluate the shear properties, minimizing the span-depth ratio of the specimen is essential. Additionally, the distance between the reaction bearing plate and the load-bearing blocks should typically be at least twice the specimen depth. Therefore, glulam beams with dimensions of 370 mm (L) \times 55 mm (W) \times 80 mm were tested under bending with a single vertical load applied at the mid-span, in accordance with ASTM D198-15 (ASTM International, 2015), at a span-depth ratio of 2. Bending tests were conducted using a universal testing machine (UTM4304, SUNS, China) with a loading rate of 5 mm/min until failure. Fig. 6 presents a schematic diagram of the bending test setup, including the locations of the linear variable differential transformer (LVDT) and strain gauges. The deflection values recorded by the LVDT were used to calculate the initial stiffness using PickPoint software (v. 3.2.4). The software employs a bi-linear approximation model to determine the initial stiffness by calculating the slope of the linear portion of the load-displacement curve, representing the elastic region.

2.4.2. Analytical methods for shear strength

Because the untreated and densified Chinese fir have different moduli in the principal axis of bending, the composite glulam beams can be treated as beams of different materials according to the elementary

beam theory. This can be dealt with by using an equivalent width technique, in which the width of each component parallel to the principal axis of bending is proportional to the modulus of elasticity (MOE) of the component material (Huang et al., 2023). For composite glulam beams, the equivalent width of densified laminates can be determined by Eq. (6). The MOE of untreated Chinese fir E_u set at 7500 MPa and of densified Chinese fir E_d set at 12,000 MPa (Ma et al., 2023). Fig. 7 shows the cross section of normal and composite glulam beams with width b and b_r , respectively.

$$b_r = \frac{E_d}{E_u} b \quad (6)$$

Where b_r is the equivalent width of densified laminates, in mm; E_d is the MOE of densified Chinese fir, and E_u is the MOE of untreated Chinese fir.

The shear stress in the different effective depth of the composite glulam beams can be calculated by Eq. (7).

$$\tau_y = \frac{VS_{z(y)}}{I_{eq}b} \quad (7)$$

Where: τ_y is the shear stress at a distance of y from the neutral axis on the cross-section, in MPa; V is the maximum shear force, in kN; $S_{z(y)}$ is the first moment of equivalent area below the line parallel to the neutral axis at y , in mm^3 . I_{eq} is the moment of inertia of the equivalent cross-section, in mm^4 .

The shear stress achieves maximum value at the neutral axis, calculated according to Eq. (8), which is called the composite beam equation in this study. At this point, the theoretical shear capacity of the composite beam is calculated using Eq. (9).

$$\tau_{max} = \frac{VS_z}{I_{eq}b} \quad (8)$$

Where τ_{max} is the maximum shear stress, in MPa; S_z is the first moment of the equivalent area below the neutral axis.

$$F_{v,cal} = 2 \frac{I_{eq}b}{S_z} \tau \quad (9)$$

For normal glulam beams, the maximum shear stress calculated by Eq. (10) according to ASTM D198-2015 (ASTM D 198-15, 2015), which is called homogeneous beam equation in this study.

$$\tau_{max} = \frac{3P}{4bh} \quad (10)$$

Where: P is the maximum shear force, and b and h are the breadth and depth of the specimen, respectively, in mm.

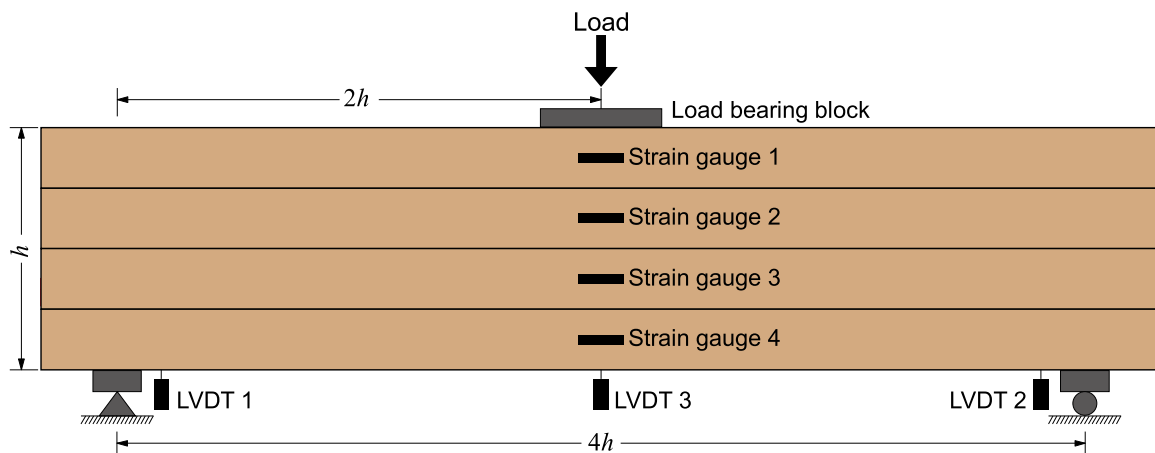


Fig. 6. Schematic diagram of shear test loading and measuring point layout of glulam short beams.

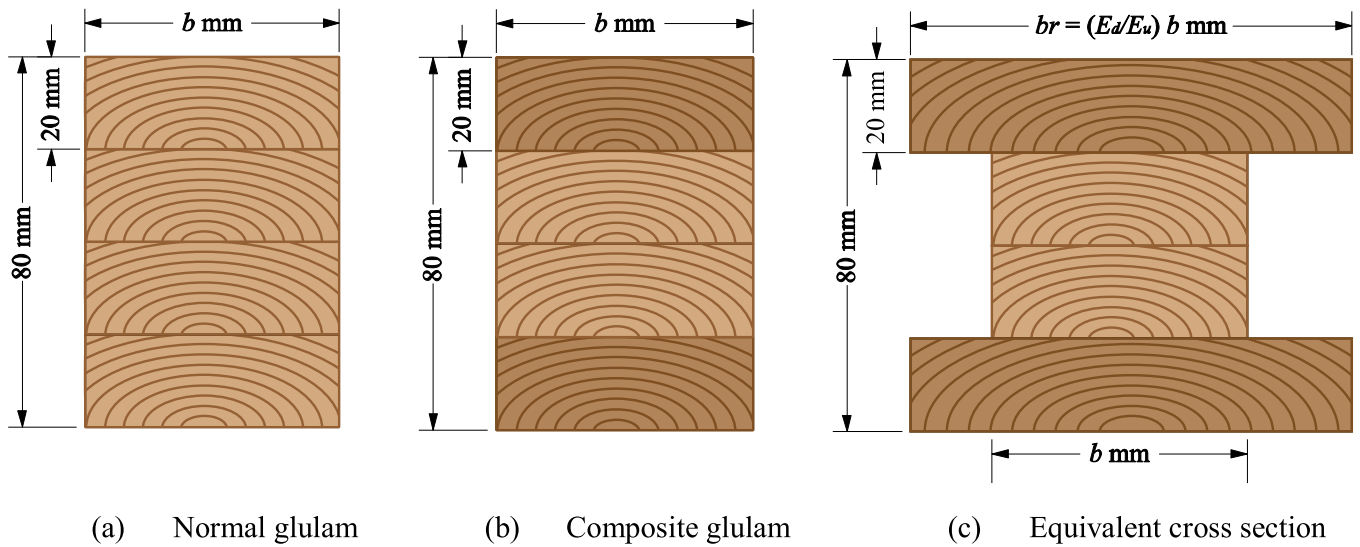


Fig. 7. Equivalent cross section for normal and composite glulam beams.

3. Results and discussion

3.1. Bonding performance analysis

3.1.1. Delamination test results

The bonding performance of structural glulam is critical for its durability and structural safety. Fig. 8 presents the delamination test results for composite and normal glulam. The results showed that all specimens exhibited good bonding strength during the first soaking and boiling cycles, with delamination rates below 5 %. However, in the second cycle, severe delamination occurred in specimen 1 during the soaking test and specimen 2 during the boiling test of the untreated glulam group, with delamination rates of 17.95 % and 15.47 %, respectively. In contrast, the delamination rates of all composite glulam specimens remained below 5 %, with the maximum delamination less than 25 % of the length of a single glue-line, meeting the GB/T 26899-2022 standards. This confirms that the composite glulam satisfies the durability requirements for glue-lines, making it suitable for use in outdoor environments with high humidity.

Besides, typical failure modes illustrated in Fig. 9, included delamination at the glue-line or cracking within the wood along the



Fig. 9. Typical failure mode of delamination test.

longitudinal direction, suggesting that the glue-line strength surpassed that of the wood.

Composite glulam exhibited superior bonding durability compared to untreated glulam, aligning with the findings of Hajihassani et al. (2022). However, this contrasts with the findings of Nandika et al. (2021), who reported better bonding in non-densified glulam due to its lower density and higher porosity. The discrepancy with Nandika's

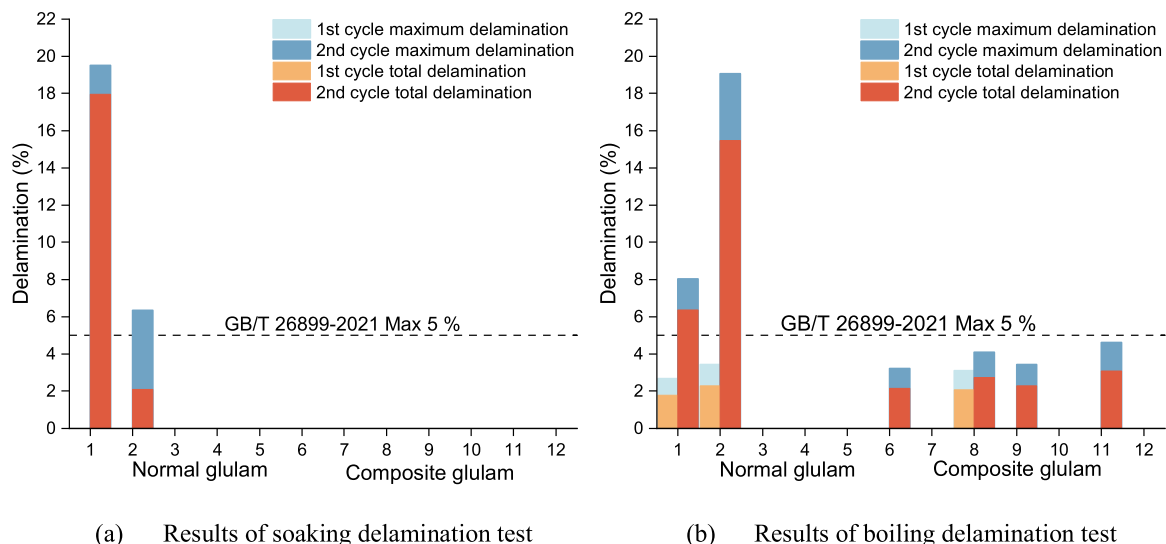


Fig. 8. Results of delamination test for normal and composite glulam.

findings can be attributed to the pre-heating treatment that changing the mechanical and chemical properties of densified wood, which was not reported by Nandika's study. Mechanically, the yield stress of the wood was significantly reduced (Scharf et al., 2023), which was the result of the softening of the wood components including amorphous regions of cellulose, hemicellulose, and lignin under the influence of hydrothermal when be heated at a temperature of 120 °C, with a relatively high moisture content of 50 %. Chemically, one of the main changes was the hydrolysis of hemicellulose, as it is more sensitive to temperature, particularly at high moisture contents (Gao, 2024). This hydrolysis weakens the bonds between the microfibrils and lignin, reducing the internal stresses accumulated during the compression process (Srivaro et al., 2022). Additionally, the lignin undergoes fragments and condensation reactions. The cleavage of β -O-4' aryl ether linkage in the lignin backbone exposed more active sites on lignin aromatic ring that facilitate the formation of new C-C bonds (Zhang et al., 2017), which reduce the number of free hydroxyl groups, decreasing hydrophilicity and increasing hydrophobicity (Yin et al., 2011). Moreover, plasticization of lignin leads to a reorganization of the lignocellulosic components, which also reduces wood's wettability (Hakkou et al., 2005). These combined mechanical and chemical changes significantly reduce the hygroscopicity of wood and the internal stresses, thereby enhancing the dimensional stability of the wood. Additionally, the pre-heating treatment contributes to the surface densified wood becoming compact and smooth, which allows the adhesive to flow more evenly over the surface (Liu et al., 2018). As a result, the bonding performance of composite glulam during the soaking and boiling delamination tests was improved, explaining the observed differences compared to Nandika's results. This highlights the critical role of the hydro-thermal effects in improving bonding performance.

Furthermore, the presence of microcracks, which inevitably form during the compression process, positively affect adhesive penetration and the formation of mechanical junctions, further enhancing the bonding performance (Hajihassani et al., 2022). As shown in Fig. 10, SEM analysis demonstrates that cell wall breakages and cracks are predominantly observed in latewood regions, where tangential microcracks within the latewood tracheids increase adhesive penetration depths into the densified wood (Mamonova et al., 2022). In contrast, earlywood exhibits less obvious breakage due to its thinner cell walls, while the lumens remain partially open, preserving some porosity and allowing the adhesive to infiltrate effectively.

3.1.2. Glue-line shear strength

Fig. 11 presents the glue-line shear test results for composite and

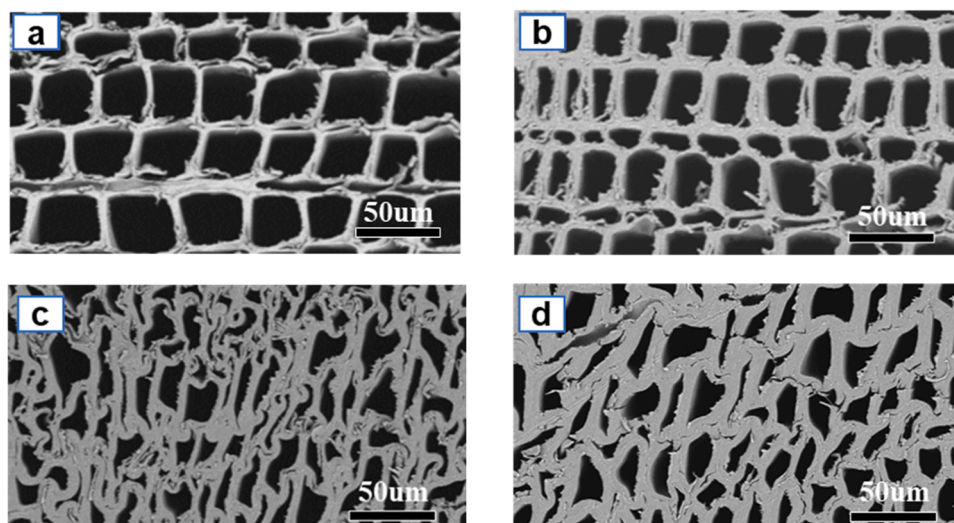


Fig. 10. SEM images of untreated Chinese fir early wood (a), latewood (b) and densified Chinese fir early wood (c), latewood (d).

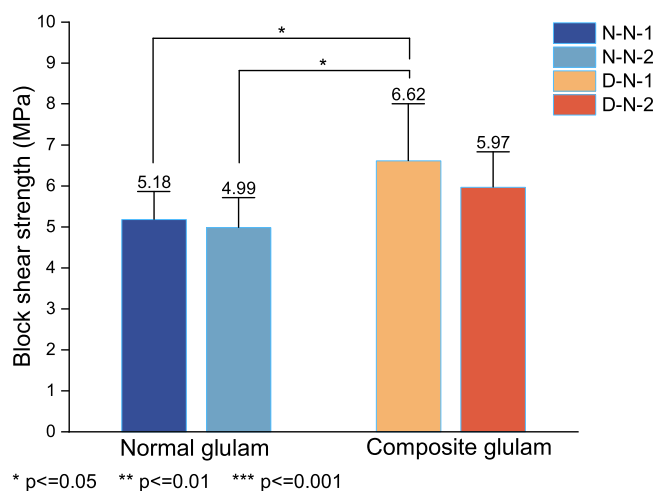


Fig. 11. Block shear strength of two types of glulam.

normal glulam. The composite glulam exhibited enhanced glue-line shear strength compared to normal glulam. Specifically, the D-N-1 group, representing the glue-line between the outer and inner laminates of composite glulam, showed a mean shear strength of 6.62 MPa, which was 18.6 %, 27.8 %, and 32.7 % higher than the D-N-2, N-N-1, and N-N-2 groups, respectively. The Shapiro-Wilk test was conducted to assess the normality of each data group, and the results indicated that all groups followed a normal distribution at a 0.05 significance level. Additionally, Levene's test for homogeneity of variances showed p-values greater than 0.05 for all groups, confirming equal variance. Based on these conditions, independent-sample t-tests were performed. The results revealed a significant difference in shear strength between the N-N-1 and N-N-2 glue-lines compared to the D-N-1 glue-line, with $P = 0.045$ and $P = 0.028$ respectively. Although the difference between the N-N-2 and D-N-2 glue-lines did not reach statistical significance, it approached it with $p = 0.056$. The t-test results further demonstrate that densification of laminates significantly enhances glue-line shear strength. The shear strength values of individual glue-lines and the average of all glue-lines in composite glulam met the GB/T 26899 standard, while the normal glulam failed to meet the required average shear strength of 6 MPa.

The average wood failure percentages of two types of glulam ranged from 85.25 % to 99.19 %, as shown in Fig. 12. Although the D-N-1 group exhibited a relatively lower average wood failure percentage, it still met

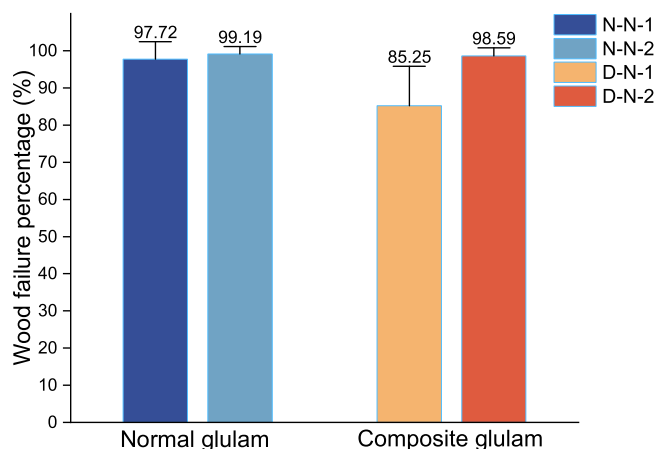


Fig. 12. Wood failure percentage of two types of glulam.

the requirement of GB/T 26899, which specifies that the average wood failure percentage must be $\geq 144 \cdot (9f_v)$.

Fig. 13 shows the failure mode observed in all specimens was shear failure in the wood near the glue-line. The increased shear strength of composite glulam can be attributed to the enhanced mechanical properties of the densified laminates. The observed failure modes and higher wood failure percentage indicate that failure primarily occurred in the wood rather than in the glue-line itself, suggesting that the glue-line strength exceeded that of the wood. Consequently, the overall shear performance of the glulam was predominantly determined by the shear strength of laminates. The densification process increased the density and mechanical resistance of the laminates, which contributed to the improved shear strength of composite glulam (Faircloth et al., 2024; Vnućec et al., 2017). Moreover, the enhancement in glue-line shear strength due to the increased density could be found in another important EWPs, cross laminated timber (CLT). The CLT specimens manufactured using densified batai wood with compression rate of 50 % shows significant enhancement in glue-line shear strength compared with untreated CLT (Liew et al., 2022), suggesting that densification not only positively affect bonding quality of glulam but other wood



(a) N-N-2 Group from normal glulam



(b) D-N-1 Group from composite glulam

Fig. 13. Typical failure mode of the specimen.

composites.

3.2. Shear performance of glulam short beams

3.2.1. Failure mode

The dominant failure mode observed in the untreated glulam specimens was shear failure localized in the bottom laminates. Cracks initiated in the bottom laminates near the inner side of the supports and then propagated along the beam length towards the middle layers. This failure mode can be attributed to stress concentration at the contact area between the wood and the support. Despite the intentional increase in the contact area of the supports, the low density and compressive strength of untreated Chinese fir led to significant localized compressive deformation, which further intensified the stress concentration. Consequently, due to the relatively low shear strength of untreated Chinese fir, oblique shear failure developed near the supports as the shear force reached its maximum in this region. In addition to the shear failure observed at the bottom layers, one specimen experienced bending failure characterized by tensile rupture of the wood fibers at the bottom surface. This bending failure occurred under the combined influence of bending moments and shear forces, causing cracks to propagate diagonally upward towards the glue-line interface. The typical failure patterns, including shear failure at the support regions and bending-induced tensile cracking, are illustrated in Fig. 14.

Fig. 15 illustrates the typical failure mode of composite glulam. In composite glulam specimens, shear failure was the predominant mode of failure, but the locations of crack initiation varied. The most common failure pattern involved cracks initiating near the neutral axis, where diagonal cracks first developed in the middle laminates, leading to shear failure. These cracks then propagated along the length of the beam towards the ends. This behavior can be attributed to the increased density and compressive strength of the outer laminates after densification, which significantly reduced localized compressive deformation at the contact points between the wood and supports, thereby minimizing stress concentration effects. Additionally, the higher shear strength of the densified Chinese fir made the outer layer of the composite beam less susceptible to shear failure. Consequently, diagonal cracks were more likely to initiate near the neutral axis, where shear stress reaches its maximum. This change in failure mode is significant for the structural application of Chinese fir glulam, as the current structural design methods assume that shear failure occurs at the neutral axis, where shear stress is predicted to be greatest according to simple beam theory. This assumption is used to determine the design shear strength, which is typically set higher than the calculated shear strength to ensure structural safety. However, if a glulam beam experiences diagonal shear failure near the supports, rather than at the neutral axis, the actual shear capacity could be considerably lower than the design shear strength. This discrepancy could introduce potential risks when applying these beams in large-scale structural applications.

In specimen DGL3, failure occurred at a point one-quarter of the height from the bottom of the beam, where interlaminar shear displacement developed along the wood fibers from the mid-span to the

ends. This was mainly due to the significant difference in mechanical properties between the densified outer laminates and the untreated inner laminates, creating a notable stress differential at their interface.

Additionally, microcracks in the latewood compromised the wood original structure, creating weak zones that may lead to stress concentrations and reduce load transfer efficiency. As a result, shear failure could occur at the outer laminates, rather than near the neutral axis as predicted by conventional beam theory. This potential risk highlights the need to optimize pre-heating and densification parameters to minimize cell wall breakage.

3.2.2. Shear strength

Fig. 16 presents the load-deflection curves for both normal and composite glulam beams, indicating a progressive shear damage process. After the appearance of the first crack, the load decreased slightly, then gradually increased until it sharply dropped upon complete failure, demonstrating a certain degree of ductility, as seen in the typical curves of specimens GL4, DGL1, and DGL4. Compared to normal glulam beams, composite glulam beams exhibited higher elastic ultimate loads and deflections, with some specimens achieving an elastic ultimate deflection exceeding 2 mm. This behavior can be attributed to the enhanced mechanical properties and stiffness achieved through the densification of the outer laminates. Table 1 shows the initial stiffness of glulam beams. The average initial stiffness of the composite glulam was 10.23 kN/mm, an increase of 13.67% over normal glulam beams. This improvement corresponds with the steeper slope observed in the elastic region of the load-displacement curves, highlighting the enhanced stiffness of the composite glulam.

Specimen GL1 from the normal glulam group exhibited tensile failure rather than shear failure, and specimen DGL3 from the composite glulam group showed interlaminar displacement between the outer and inner layers, resulting in a very low maximum shear force. Therefore, the results of GL1 and DGL3 were excluded from the analysis. For the remaining specimens, the maximum shear strength was calculated using Eq. (10). To further evaluate the performance of the composite glulam beams, the maximum shear strength was recalculated using the composite beam equation. The equivalent width of densified outer laminates was determined according to Eq. (6). Based on this effective width, the shear strength was then calculated using Eq. (8). The results are summarized in Table 1.

For composite glulam beams, the shear strength calculated using the composite beam equation was approximately 92.69–94.94% of that obtained using the homogeneous beam equation, consistent with findings from previous studies (Ido, 2009). Therefore, a comparison was made between the shear strength of normal glulam beams calculated using the homogeneous beam equation and that of composite glulam beams calculated using the composite beam equation. The average maximum shear force and shear strength of composite glulam beams increased by 31.95% and 21.51%, respectively, compared to normal glulam beams. This suggests that the densification of the outer laminates in Chinese fir glulam positively contributes to enhancing shear strength under bending tests.



Fig. 14. The typical failure modes of normal Chinese fir glulam.

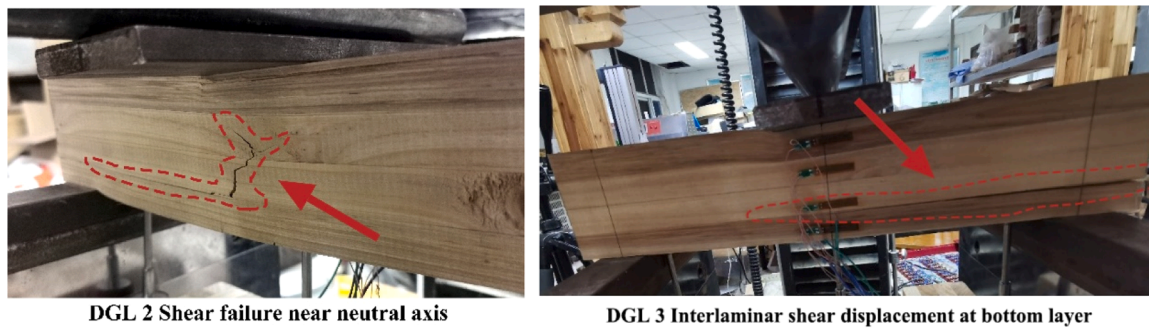


Fig. 15. The typical failure modes of composite Chinese fir glulam.

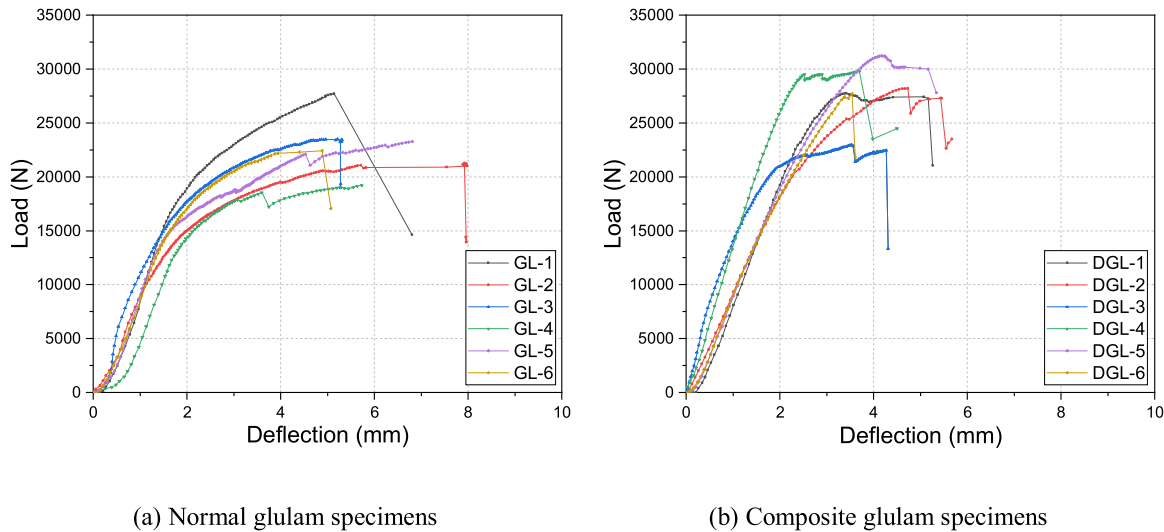


Fig. 16. Load-midspan deflection curve.

Table 1
Shear strength calculated from homogeneous beam equation and composite beam equation.

Glulam type	Initial Stiffness (kN/mm)	Maximum shear force (kN)	Shear strength (N/mm ²)	
			Homogeneous beam equation	Composite beam equation
Normal (n = 5)	9.00 (13.24)	21.95 (7.95)	3.99 (6.57)	-
Composite (n = 5)	10.23 (18.45)	28.96 (5.23)	5.17 (4.91)	4.85 (4.51)

Note. Values represent the mean result followed by the coefficient of variation (CV) in parentheses.

3.2.3. Shear stress distribution

Fig. 17 illustrates the maximum shear stress values along the beam thickness for both normal and composite glulam. In both types of glulam, the maximum shear stress occurs in the middle layer. The shear stress distribution in normal glulam beams follows a parabolic pattern, whereas in composite glulam, the shear stress is relatively low in the outer layers and then suddenly increases at the interface between the outer and inner layers. This indicates that the middle layers bear most of the shear stress.

The distribution of shear stress helps explain why specimen DGL3 in the composite glulam group exhibited interlaminar displacement and shear failure at a point one-quarter of the height from the bottom of the beam. It is evident that the densification of the outer laminates in glulam alters the shear stress distribution, resulting in a pattern similar to that of

I-beams in composite glulam beams. In this configuration, the middle two laminates of untreated Chinese fir function similarly to the web plate of an I-beam, primarily bearing the shear forces. Moreover, the sudden and significant increase in shear stress between the outer and inner layers highlights the need to prevent interlaminar displacement at this location, as it could lead to premature failure of the glulam beam.

3.2.4. Calculation of theoretical shear capacity

Based on the theory of composite beams, the equivalent length of the densified outer laminates in composite glulam was calculated using Eq. (6). The shear stress distribution of the composite glulam beam resembles that of an I-beam, with the shear force primarily borne by the untreated Chinese fir in the middle layers. Correspondingly, the predominant failure mode for composite glulam beams was shear failure within the untreated Chinese fir in these middle layers. Thus, the shear strength of normal glulam beams, as calculated using Eq. (10), was applied to estimate the theoretical shear capacity of the composite glulam beams according to Eq. (9). The results are presented in Table 2.

The theoretical shear capacity is lower than the experimental shear capacity, ranging from approximately 79–87 % of the experimental values. This deviation might be attributed to the difference in failure modes: normal glulam primarily exhibits oblique shear failure near the supports rather than shear failure near the neutral axis, leading to a lower observed shear strength. Using this lower value as the shear strength of the middle layer in composite glulam beams for calculating the overall shear capacity of the composite beam ultimately resulted in theoretical values that are slightly lower than the experimental values.

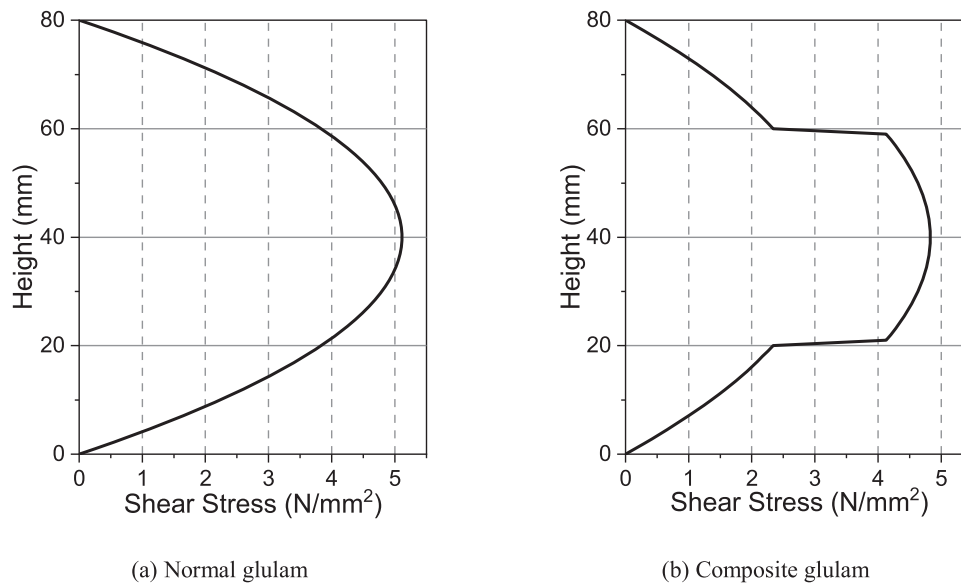


Fig. 17. Shear stress distribution over the cross section of each glulam at 30 kN load.

Table 2
Results of theoretical shear capacity calculation.

Code	Width (mm)	Height (mm)	I_z (mm ⁴)	S (mm ³)	F_v (kN)	$F_{v,cal}$ (kN)	Error (%)
DGL1	53.76	76.92	3,341,131	60,814	27.77	23.37	-15.83
DGL2	54.13	77.65	3,452,873	62,871	28.21	23.55	-16.50
DGL4	54.06	77.07	3,371,065	60,163	29.79	23.91	-19.73
DGL5	54.65	77.90	3,524,844	63,019	31.24	24.17	-22.63
DGL6	54.26	78.48	3,578,471	63,538	27.82	24.17	-13.15

4. Conclusion

This study verified the feasibility of fabricating composite glulam using densified Chinese fir and untreated fir, the main findings can be summarized as follows:

- (a) The glue-line delamination tests indicated that composite glulam exhibited superior bonding durability, which can primarily be attributed to the enhanced dimensional stability of the densified laminates. This improvement in stability resulted from hydro-thermal effects during pre-heating, which induced both mechanical and chemical changes in the wood structure, thereby reducing moisture-induced dimensional changes during wet-dry cycling. Additionally, microcracks created during the compression process further enhanced adhesive penetration and mechanical interlocking, contributing to improved bonding durability. These combined effects enabled the composite glulam to meet the requirements of GB/T 26899-2022, demonstrating its suitability for use in outdoor environments with high humidity.
- (b) The densification of outer laminates significantly enhanced glue-line shear strength through increased density and mechanical properties. The improvement in interfacial bonding strength was achieved while maintaining high wood failure percentages, demonstrating that the adhesive bond strength exceeded the intrinsic strength of the wood material, ensuring reliable structural performance.
- (c) The composite glulam design improved overall beam shear strength by reducing stress concentration near the supports through densified outer laminates, preventing premature diagonal shear failure in these regions. The observed failure patterns indicated typical shear behavior, with most failures occurring near the neutral axis. This suggests that the composite structure

effectively redistributes shear stresses, though variations in stress distribution across different laminate layers should be considered in future structural designs. These findings demonstrate the potential of selectively densified composite glulam for enhanced structural applications.

CRediT authorship contribution statement

Panpan Ma: Writing – original draft. **Jianzhang Li:** Supervision. **Jinqiu Xie:** Data curation. **Zeli Que:** Writing – review & editing, Supervision. **Xin An:** Investigation. **Bin Zhou:** Data curation. **Shuo Wang:** Methodology. **Xinran Li:** Investigation.

Declaration of Competing Interest

The authors declare that they have no known competing financial interests or personal relationships that could have appeared to influence the work reported in this paper.

Acknowledgments

This work was supported by National Key Technology Research and Development Program for the 14th Five-year Plan of China (2024YFD2201204).

Data availability

Data will be made available on request.

References

- D198-15, 2015. Standard Test Methods of Static Tests of Lumber in Structural Sizes. ASTM International.

- Faircloth, A., Gilbert, B.P., Kumar, C., Leggate, W., McGavin, R.L., 2024. Understanding the adhesion performance of glued laminated timber manufactured with Australian softwood and high-density hardwood species. *Eur. J. Wood Wood Prod.* 82 (6), 2013–2028. <https://doi.org/10.1007/s00107-024-02138-3>.
- Franke, S., Franke, B., Harte, A.M., 2015. Failure modes and reinforcement techniques for timber beams – state of the art. *Constr. Build. Mater.* 97, 2–13. <https://doi.org/10.1016/j.conbuildmat.2015.06.021>.
- Gao, Z., 2024. Wood sandwich softening behavior via coupling of moisture and heat. *Constr. Build. Mater.* 428, 136396. <https://doi.org/10.1016/j.conbuildmat.2024.136396>.
- Hajihassani, R., Ghahri, S., Masoomeh Zamani, S., Nourbakhsh, A., 2022. Performance of densified wood glulam as building bio-material. *J. Renew. Mater.* 10 (2), 511–526. <https://doi.org/10.32604/jrm.2022.017781>.
- Hajihassani, R., Ghahri, S., Zamani, S.M., Nourbakhsh, A., 2021. Performance of densified wood glulam as building bio-material. *J. Renew. Mater.* 10 (2), 511–526. <https://doi.org/10.32604/jrm.2022.017781>.
- Hakkou, M., Pétrissans, M., Zoulalian, A., Gérardin, P., 2005. Investigation of wood wettability changes during heat treatment on the basis of chemical analysis. *Polym. Degrad. Stab.* 89 (1), 1–5. <https://doi.org/10.1016/j.polymdegradstab.2004.10.017>.
- Harte, A.M., 2017. Mass timber – the emergence of a modern construction material. *J. Struct. Integr. Maint.* 2 (3), 121–132. <https://doi.org/10.1080/24705314.2017.1354156>.
- Huang, Z., Jiang, L., Ni, C., Chen, Z., 2023. The appropriacy of the analytical models for calculating the shear capacity of cross-laminated timber (CLT) under out-of-plane bending. *J. Wood Sci.* 69 (1), 14. <https://doi.org/10.1186/s10086-023-02089-y>.
- Ido, H., Nagao, H., Kato, H., Yoshida, N., 2009. Shear tests of glulam with different lamina compositions failure modes and shear strength. *Mokuzai Gakkaishi* 55 (5), 316–321. <https://doi.org/10.2488/jwrs.55.316>.
- Kong, F., Zhou, B., An, X., Wang, F., Wang, S., Ma, P., Que, Z., 2024. Experimental investigation on mechanical properties of Chinese fir composites as cross-laminated timber. *Ind. Crops Prod.* 213, 118411. <https://doi.org/10.1016/j.indcrop.2024.118411>.
- Kutnar, A., Sandberg, D., Haller, P., 2015. Compressed and moulded wood from processing to products. *Holzforschung* 69 (7), 885–897. <https://doi.org/10.1515/hf-2014-0187>.
- Liew, K.C., Tan, Y.F., Albert, C.M., Raman, V., 2022. Cross-laminated timber and glulam from low-density *Paraserianthes falcataria*: a look into densification and shear strength. *J. Wood Sci.* 68 (10), 1540. <https://doi.org/10.3390/fl3101540>.
- Liu, H., Shang, J., Kamke, F.A., Guo, K., 2018. Bonding performance and mechanism of thermal-hydro-mechanical modified veneer. *Wood Sci. Technol.* 52 (2), 343–363. <https://doi.org/10.1007/s00226-017-0982-x>.
- Ma, P., An, X., Wang, F., Huang, H., Chen, Z., Wang, S., Gong, M., Que, Z., 2023. Effects of pre-heating treatment parameters on dimensional stability and mechanical properties of densified Chinese fir. *Constr. Build. Mater.* 407, 133484. <https://doi.org/10.1016/j.conbuildmat.2023.133484>.
- Mamonova, M., Ciglian, D., Reinprecht, L., 2022. SEM analysis of glued joints of thermally modified wood bonded with PUR and PVAc glues. *Materials (Basel)* 15 (18). <https://doi.org/10.3390/ma15186440>.
- Ministry of Housing and Urban-Rural Development of the People's Republic of China, 2012. GB/T 50329-2012. Standard for Test Methods of Timber Structures. China Architecture & Building Press, Beijing, China.
- Nandika, D., Darmawan, I.W., Karlinasari, L., Hadi, Y.S., Abdillah, I.B., Putri, J.Y., 2021. Physical-mechanical properties and durability enhancement of glued laminated lumber made from inner part of *Corypha utan* Lam. Trunk: the effect of lamina densification and lumber smoking. *Bioresources* 16 (4), 8320–8337. <https://doi.org/10.15376/biores.16.4.8320-8337>.
- National Forestry and Grassland Administration, 2019. China Forest Resource Report 2014–2018. China Forestry Publishing House, Beijing, China.
- Ou, J.J., Zhang, Y., Long, W., Chen, D., Zhong, Y., 2023. Bending properties of glulam made by domestic fast-growing Chinese fir. *J. Build. Mater.* 26 (12). <https://doi.org/http://kns.cnki.net/kcms/detail/31.1764.TU.20230602.1840.030.html>.
- Paul, B.N., Shukla, S.R., Kelkar, B.U., Nagraik, P., 2024. Production processes, material properties and applications of densified wood: an overview. *J. Indian Acad. Wood Sci.* 21 (2), 235–254. <https://doi.org/10.1007/s13196-024-00348-z>.
- Scharf, A., Lemoine, A., Neyses, B., Sandberg, D., 2023. The effect of the growth ring orientation on spring-back and set-recovery in surface-densified wood. *Holzforschung* 77 (6), 394–406. <https://doi.org/10.1515/hf-2023-0004>.
- Söğütlü, C.J.B., 2017. Determination of the effect of surface roughness on the bonding strength of wooden materials. *Bioresources* 12, 1417–1429. <https://doi.org/10.15376/BIORES.12.1.1417-1429>.
- Sotayo, A., Bradley, D., Bather, M., Sareh, P., Oudjene, M., El-Houjeyri, I., Harte, A.M., Mehra, S., O'Ceallaigh, C., Haller, P., Namari, S., Makradi, A., Belouettar, S., Bouhala, L., Deneufbourg, F., Guan, Z., 2020. Review of state of the art of dowel laminated timber members and densified wood materials as sustainable engineered wood products for construction and building applications. *Dev. Built Environ.* 1, 100004. <https://doi.org/10.1016/j.dibe.2019.100004>.
- Srivaro, S., Lim, H., Li, M., Altaner, C., 2022. Effect of pressing parameters on dimensional stability and bonding performance of thermally compressed coconut wood. *Constr. Build. Mater.* 357, 129359. <https://doi.org/10.1016/j.conbuildmat.2022.129359>.
- Standardization Administration of China, 2021a. GB/T 1927.5-2021. Test Methods for Physical and Mechanical Properties of Small Clear Wood Specimens-Part 5: Determination of density. Standards Press of China, Beijing, China.
- Standardization Administration of China, 2021b. GB/T 1927.4-2021. Test Methods for Physical and Mechanical Properties of Small Clear Wood Specimens-Part 4: Determination of Moisture Content. Standards Press of China, Beijing, China.
- Standardization Administration of China, 2022. GB/T 26899-2022. Structural Glued Laminated Timber. Standards Press of China, Beijing, China.
- Vnučec, D., Žigon, J., Mikuljan, M., Kamke, F.A., Šernek, M., Kutnar, A., Goršek, A., 2017. Bonding of densified beech wood using adhesives based on thermally modified soy proteins. *Eur. J. Wood Wood Prod.* 75 (5), 767–776. <https://doi.org/10.1007/s00107-017-1164-0>.
- Wang, X., Que, Y., Hu, Y., Jiang, G., Que, Z., 2018. Effect of different thickness of the layers of cross-laminated timber made from Chinese fir on the mechanical performance. *Bioresources* 13 (3), 7002–7016. <https://doi.org/10.15376/biores.13.3.7002-7016>.
- Wang, J., Wang, X., Zhan, T., Zhang, Y., Lv, C., He, Q., Fang, L., Lu, X., 2018. Preparation of hydro-thermal surface-densified plywood inspired by the stiffness difference in “sandwich structure” of wood. *Constr. Build. Mater.* 177, 83–90. <https://doi.org/10.1016/j.conbuildmat.2018.05.135>.
- Wang, J.B., Wei, P., Gao, Z., Dai, C., 2018. The evaluation of panel bond quality and durability of hem-fir cross-laminated timber (CLT). *Eur. J. Wood Wood Prod.* 76 (3), 833–841. <https://doi.org/10.1007/s00107-017-1283-7>.
- Yin, Y., Berglund, L., Salmén, L., 2011. Effect of steam treatment on the properties of wood cell walls. *Biomacromolecules* 12 (1), 194–202. <https://doi.org/10.1021/bm101144m>.
- Zhang, Y., Wu, J.-Q., Li, H., Yuan, T.-Q., Wang, Y.-Y., Sun, R.-C., 2017. Heat treatment of industrial alkaline lignin and its potential application as an adhesive for green wood–lignin composites. *ACS Sustain. Chem. Eng.* 5 (8), 7269–7277. <https://doi.org/10.1021/acssuschemeng.7b01485>.